Wear simulation for boundary lubricated, radially loaded, spherical roller bearings

Cameron D. Milne[1] and Paul A. Meehan[1]

[1]School of Mechanical & Mining Engineering, The University of Queensland, Brisbane, Australia

ABSTRACT

The wear of railway axle bearings is an important phenomenon. Rail companies must keep their rolling stock in a serviceable condition as excessively worn bearings can contribute to safety issues such as vibrations, excessive clearances and possibly even derailments. At present, maintenance scheduling is typically performed at predetermined time intervals. Predicting the wear and degradation of the bearings, would enable operators and bearing manufacturers to 1) optimise the design and maintenance of the bearings, and 2) quantitatively determine the best time to replace the bearings. This paper presents a model developed for predicting the wear in radially loaded spherical roller railway axle bearings. It uses a slice method to calculate the roller load, traction and creep distribution along the roller for the contact mechanics, and predicts wear using a frictional power model. The model is first validated with the wear in a thrust bearing in the literature and then used to predict wear in the radial bearing. The wear contribution from each roller in the loading zone due to the radial loading is calculated and combined for an overall wear profile.

1. INTRODUCTION

The wear and degradation of railway axle bearings poses a great cost to the rail industry. The sheer number of rolling stock and the physical demands needed to overhaul a single bearing means that replacing the axle bearings is a big task, and costs the operators in the order of millions of dollars to service a single fleet of trains. In the literature, there have been several contributions which relate to the issue at present: Modelling of a spherical roller thrust bearing in the mild wear stage was successfully performed by Olofsson et al (Olofsson, Andersson, and Bjorklund 2000). This forms the central part of this paper. In other work, Nilsson et al (Nilsson, Svahn, and Olofsson 2006) counted the number of scratches from diamond particles on the contacting surfaces of a bearing and then attempted to predict the wear after a much longer running time. For a view on the position of wear in the overall picture of bearing damage, El-Thalji and Jantunen (El-Thalji and Jantunen 2014) provide a good introduction. There are many wear formulae in the literature. The most common is the Archard (Archard 1953) , and the frictional power wear methods, used in the study of wheel-rail contact by Meehan and Daniel (Meehan and Daniel 2008). A feedback model for wear was used by Meehan et al (Meehan et al. 2009), to simulate the wear in wheel-rail contact. This is described more in Section 2. Contact fatigue is a common failure mode for rolling element bearings, however this failure mode has not been observed in the present application with the bearings of interest in this study. The present research provides a description of the modelling processes used to determine the wear profile of a railway axle bearing (radially loaded spherical roller bearing), which may help to indicate the expected life of the bearing.

2. MODELLING

In the model, an iterative method was implemented, following the feedback loop shown in Figure 1. This feedback loop is based on that by Meehan et al (Meehan et al. 2009) . It is iterative as it calculates the wear in the bearing over time, depending on the feedback of previous worn profiles. This makes it adaptive, which is appropriate as the wear for each cycle depends on the effects of the previous wear cycles. As each iteration of the loop runs, there are several major stages of calculation.

1. The simulation starts with a new, unworn profile, then takes into account the previous wear.
2. The loading on each roller (which may depend on a dynamic condition) is calculated
3. The normal force determines the amount of frictional power generated in the sliding and slip regions of the rolling contact. The frictional power is determined by the contact mechanics. The contact mechanics for each roller is calculated based on the slice method used by Olofsson et al (Olofsson, Andersson, and Bjorklund 2000). The pressure on each slice depends on the profile of the roller and raceway, which change

as wear occurs. The changing conditions of the lubricant and the amount of third body particles present are assumed to affect the value of the friction coefficient used at this step. The amount of wear debris present is dependent on the worn volume removed from the bearing raceways.

4. The change in wear height for one iteration for each slice in the roller/raceway contact depends on the frictional power from the previous step. The value of the wear coefficient used at this step is assumed to be affected by 3rd body effects and lubricant film effects.
5. The wear height is accelerated for each slice using a single acceleration factor, which linearly scales the wear for one revolution to extend to multiple revolutions for each iteration.
6. The iteration increments, with the new iteration using the previous worn profile as a basis for the calculation of the next profile.

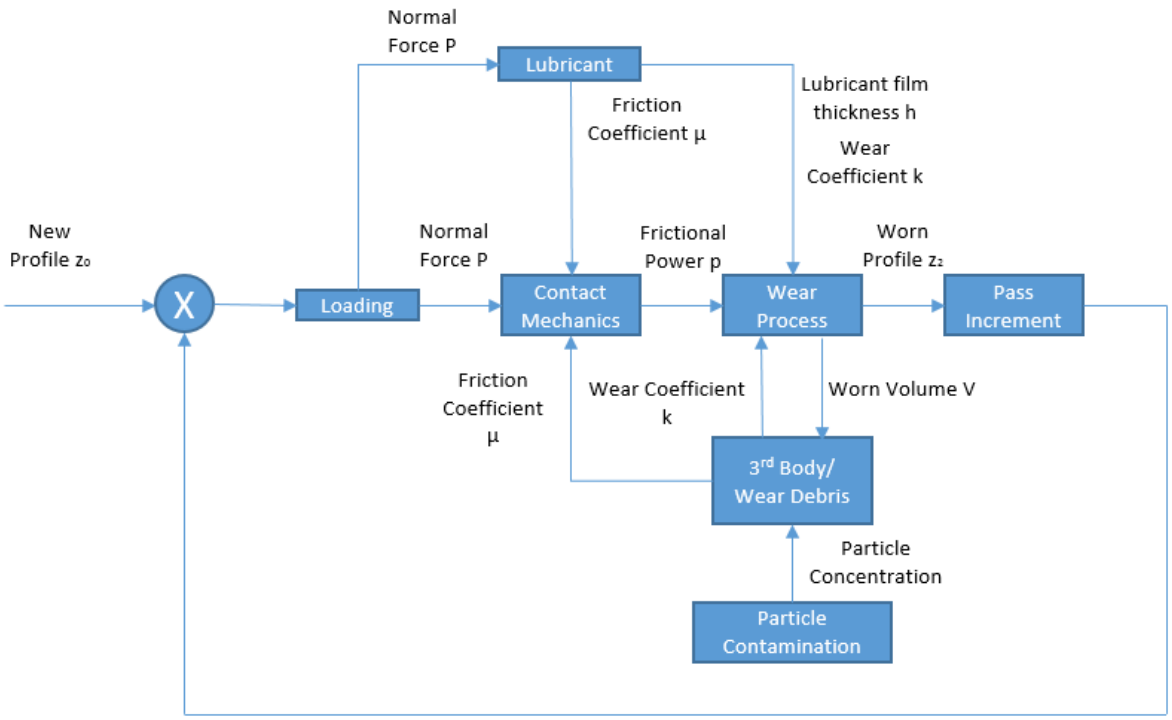

Figure 1. Feedback model for adaptive wear prediction

2.1 Thrust bearing

To develop a reliable model for the wear in a railway axle bearing (radially loaded spherical roller bearing) (the radial bearing model), the method used by Olofsson et al (Olofsson, Andersson, and Bjorklund 2000), for a spherical roller thrust bearing (the thrust bearing model), was chosen to provide a benchmark validation from the literature. Olofsson et al's (Olofsson, Andersson, and Bjorklund 2000) analysis of the thrust bearing determines the normal load in the contact between the raceway and the roller. The contact is broken up into slices perpendicular to the axis of the roller. The Palmgren (Palmgren 1959) relation for determining the normal load on a cylinder-to-cylinder contact is used, by dividing by *l* (the effective contact length), to work out the normal load per unit length at each slice. The relation for the normal load per unit length is given in Equation 1, where δ is the normal approach (how much the original circular profiles overlap), l is the effective contact length and p is the normal load per unit width. Figure 2 shows the contact broken into slices, the normal approach and the normal load applied.

$$p = \frac{\delta^{\frac{10}{9}}}{1.25 \times 10^{-5} l^{\frac{1}{9}}}$$

(1)

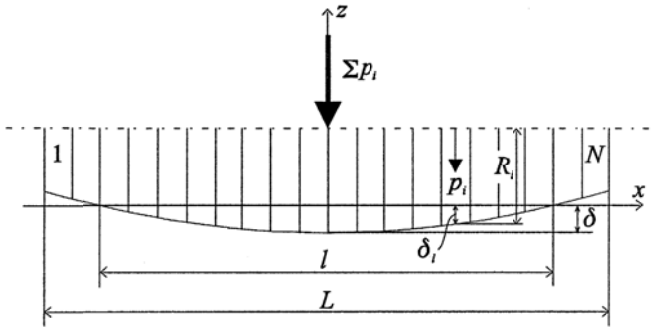

Figure 2. Cross-section of bearing roller-raceway contact. From (Olofsson, Andersson, and Bjorklund 2000); Equation 1.

Each slice of the roller has its own individual p_i, δ_i and R_i (the R_i meaning the roller radius at that slice), allowing the wear to be calculated in a 2-D manner across the contact patch. The thrust bearing model calculates the load on each slice by "pushing down" the roller profile (giving a δ_i and therefore a p_i for each slice). All the p_is are added up and multiplied by the slice width to give a total normal load (an integral). If the total normal load is insufficient for the nominal contact load, δ is increased, meaning that the total normal load increases as well. δ is increased until the nominal contact load has been achieved. In the plane going along each of these slices, the semi-contact width (the half-width of the contact patch) is given by Equation 2,

$$a_i = \left(4\frac{1-\nu}{\pi G}p_i R_i\right)^{\frac{1}{2}} \tag{2}$$

where a_i is the semi-contact width, ν is Poisson's ratio, and G is the shear modulus of the bearing material. Equations 1 and 2 are used in the calculation of the traction of the slices, in order to work out the creep profile across the roller. There is nominally no net traction transmitted within a roller-raceway contact. However, because of the geometry of the roller-raceway contacting surface, there are regions of positive and negative creep (defined as the difference in velocity of the roller and contact patch, divided by the velocity of the contact patch – a measure of sliding) away from the lines of no slip.

This creep culminates in a different traction force being applied to the roller depending on the position along the roller. Because there can be no net traction in the contact, the positive and negative traction forces (depending on the creep) must cancel. To calculate when the traction forces cancel, a "rolling cone angle" (see Figure 3 B)) is iteratively increased until the net tractional force on the roller through the contact is zero.

The rolling cone is an imaginary cone-shaped surface which intersects the curved contact at two places (these are the zero-sliding points/lines). In between the two intersection points, the creep is in one direction, and outside the two intersection points, the creep is in the opposite direction. Figure 3 B) shows a diagram of a spherical roller thrust bearing with the rolling cone illustrated, along with the direction of the creep on the roller-raceway contact, and the zero-sliding lines.

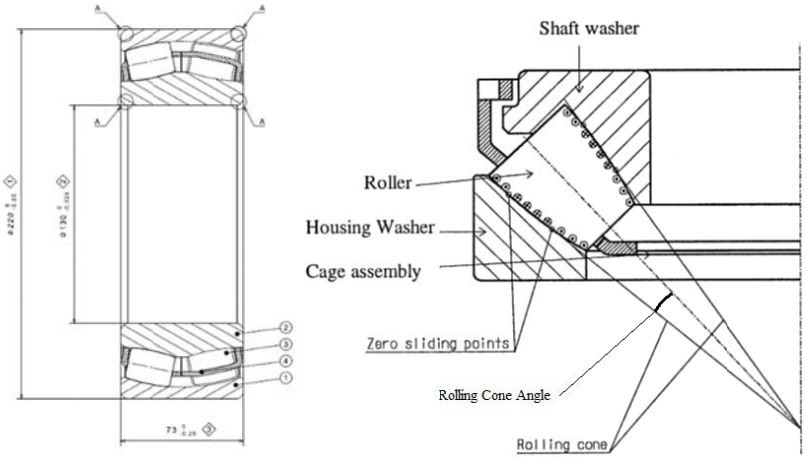

Figure 3. A) Cross-section of the railway axle bearing. B) Cross-section of a spherical roller thrust bearing showing the rolling cone, positive and negative creep and the zero sliding points. Cross in circle is the direction into the page, dot in circle is the direction out of the page. From (Olofsson, Andersson, and Bjorklund 2000)

The position of the two intersection points is determined by the rolling cone angle. The creep on each slice of the roller in the simulation is also dependent on the rolling cone angle. The rolling cone angle is found by iteratively increasing the rolling cone angle (starting with an initial guess), working out the creep and then working out the traction (then summing the total traction) for each value of the rolling cone angle. If the sum of the traction is not close to zero, the angle is increased slightly and the traction is calculated again.

The formula for the traction is from Johnson (Johnson 1960) and is given in Equation 3 i),

$$i)\ \ t_i = \mu p_i \left(1 - \left(1 + \frac{\xi_i a_i \pi G}{4\mu p_i (1-\nu)}\right)^2\right), \qquad ii)\ \ t_i = \mu p_i \tag{3}$$

where t is the traction, μ is the coefficient of friction, p is the normal load per unit length, ξ is the creep ratio, a is the semi-contact width, G is the shear modulus of the bearing material, ν is Poisson's ratio and subscript i means "for each slice". This formula holds where there is partial sliding in the contact. Where there is full sliding, the Coulomb friction relation, as in Equation 3 ii), is used.

The creep ratio ξ, is based on the actual roller radius and the rolling cone radius, as shown in Equation 4,

$$\xi_i = \frac{R_{ci} - R_{ri}}{R_{ci}} \tag{4}$$

where R_{ci} is the radius of the rolling cone for each slice, and R_{ri} is the actual radius of the roller for the corresponding slice. Once the creep profile has been established, the wear can then be calculated for each slice. The wear can now be calculated to determine the final worn profile of the raceway. The worn change in the profile height can be described by the Archard wear model as in Equation 5,

$$\Delta h_i = N_r m k p_i |\xi_i| \tag{5}$$

where h is the wear for each pass, k is a "dimensional" wear coefficient that includes the effect of hardness. N_r is the number of revolutions (an acceleration factor) and m is the number of rollers in the bearing. Over the duration of the simulation, the wear is accumulated and output as a graph on the screen. The creep gives an indication of the amount of sliding present in the contact.

The geometry used for the thrust bearing model used for validation was that for the SKF 29416 E type bearing.

2.2 Radial Bearing

Similar contact mechanics analysis to that described for the thrust bearing model was used in the model of the railway axle bearing (the radial bearing model), with some changes to incorporate the new geometry. In particular, these changes include provision that the loading is radial meaning that, depending on the position of the rollers with respect to the race ways, there will be different load contributions from the rollers at different angular positions. This means that the wear needs to be calculated at several different positions, giving a simulation of the wear in the bearing taking into account all contributions of varyingly loaded rollers.

The geometry used for the axle bearing is that for an NTN-SNR radially loaded spherical roller type bearing. It is assumed that the rollers do not suffer significant wear, and the wear is captured mostly by the raceways.

Radial Loading

The radial loading on the railway axle bearings means that the all of the load is concentrated to a few rollers at the top of the bearing, as opposed to the even load distribution in the thrust bearing model (axially loaded thrust bearing). The few rollers which carry the load all have different normal loads applied, depending on the radial clearance in the bearing (u_r) and the total radial load applied to the bearing. The wear is contributed to, by each of the loaded rollers at the top. Figure 4 shows a diagram of the load distribution in a radial roller bearing.

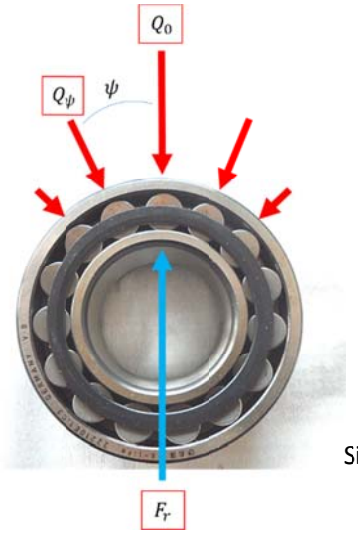

Figure 4. Diagram of the roller load distribution in a roller bearing (modified from (Wuxi Handa Bearing Co. Ltd 2016)). This figure shows that the top roller is the most highly loaded in the loaded zone.

In Figure 4, F_r is the total applied radial load to the bearing (or one side of the bearing for double-row spherical roller bearings), Q_0 is the load on the top roller, in line with and opposite to F_r. Q_ψ is the load on each of the other rollers at angle ψ to Q_0 in the loaded zone.

The method used to determine the load on each roller in the bearing is based on that found in Changsen and Zhaoying (Changsen and Zhaoying 1991). The following steps are taken in order:

1. Determine an approximate starting value for the load on the top roller (Q_0) using Equation 6 where F_r is the total radial load applied to one side of the bearing and Z is the number of rollers in one side of the bearing (for a double-row roller bearing).

$$Q_0 = \frac{4.08\,F_r}{Z} \tag{6}$$

2. Determine the maximum normal approach δ_{max} of the roller-raceway contact (this is the same as δ in Figure 2). This is calculated using the same iterative method for the normal load distribution in the thrust bearing model (where δ is incremented until the correct total normal load Q_0 is achieved).
3. Determine the load distribution factor ε from Equation 7

$$\varepsilon = \frac{1}{2}\left(1 - \frac{u_r}{2\delta_{max} + u_r}\right) \tag{7}$$

where u_r is the radial clearance in the bearing.

4. Determine $J_r(\varepsilon)$ from the lookup table in Changsen and Zhaoying (Changsen and Zhaoying 1991).
5. Determine Q_0 from Equation 8:

$$Q_0 = \frac{F_r}{ZJ_r(\varepsilon)} \tag{8}$$

The new Q_0 is different to the Q_0 determined in Step 1, and therefore δ_{max} will have changed. Therefore, Steps 2 to 5 are iterated, until Q_0 converges.

6. Once the final value of Q_0 has been found, the loads on each of the other rollers in the bearing can be obtained using Equation 9

$$Q_\psi = Q_0\left[1 - \frac{1}{2\varepsilon}(1 - cos\psi)\right]^{\frac{1}{t}} \tag{9}$$

where Q_ψ is the load on the roller at angle ψ from Q_0.t is a constant, with the value of 2/3 for a point contact (correct for a ball or spherical roller bearing).

The effect of the total radial load, F_r on the load on each roller in one half of one side of the bearing (the roller loads are symmetrical) (the number of rollers per side of the bearing, Z, is 22) is shown in Figure 5 A).

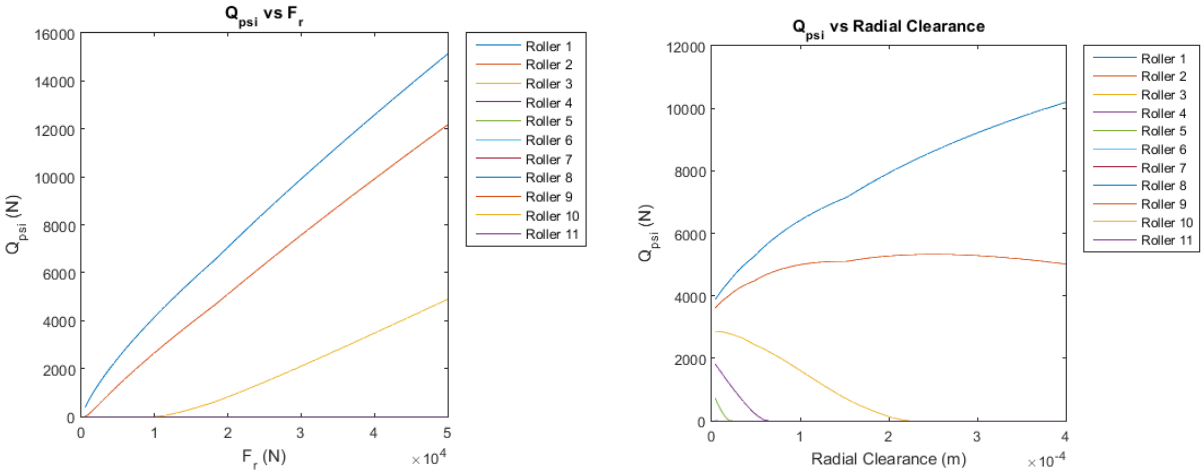

Figure 5. A) Dependence of roller load on total radial load in a spherical roller bearing. For this case, the radial clearance is 0.145 mm, B) Dependence of roller load on radial clearance in a spherical roller bearing. For this case, the bearing load is 20000 N per side of the bearing.

This figure shows that as the total radial load is increased, the load on the rollers increase, with more rollers being engaged in the loading as the load increases (e.g. Roller 3 at 1.0×10^4 N). Due to the upward radial load, the rollers in the bottom half of the bearing will always be unloaded (for rollers 6 to 11, $Q_\psi = 0$).

The effect of radial clearance on the roller loads is shown in Figure 5 B). In this plot, it can be seen that at zero radial clearance, all of the upper rollers are loaded. As the radial clearance starts to increase from zero, the load on Rollers 1 and 2 increase, while the load on rollers 3, 4, 5 and 6 all decrease. Fewer rollers are engaged in carrying the load as the radial clearance increases, indicating a more concentrated load distribution at the top of the bearing. This plot is for the spherical roller bearing with F_r = 20000 N.

When developing the thrust bearing model, the Archard wear model (Equation 10) was used to determine the wear height per slice.

$$\Delta h_i = k_1 p_i |\xi_i| \tag{10}$$

where Δh_i is the change in wear depth for each slice, k_1 is the wear coefficient, p_i is the pressure per unit length in the contact for each slice and $|\xi_i|$ is the absolute value of the creep in the contact for each slice (the absolute value is used because wear does not depend on direction).

For the radial bearing model, the frictional power wear model is used, as shown in Equation 11:

$$\Delta h = \frac{k_2 \dot{W}}{2b\rho V} \tag{11}$$

where Δh is the change in wear depth,

$$\dot{W} = Tv \tag{12}$$

is the frictional power, k_2 is the frictional power wear coefficient, $2b$ is the contact length, ρ is the bearing material density, V is the rolling velocity, T is the traction in the contact and v is the sliding velocity. Since $\frac{v}{V} = \xi$ and $\frac{T}{2b}$ is effectively the tractional load per unit length, Equation 5 can be modified for the radial bearing model, as shown in Equation 13:

$$\Delta h_i = \frac{k_2 |t_i||\xi_i|}{\rho} \tag{13}$$

where Δh_i is the change in wear depth for each slice, $|t_i|$ is the absolute value of the tractional load per unit length for each slice (from Equations 3 i) and ii)) and $|\xi_i|$ is the absolute value of the creep in the contact for each slice. The absolute values are used because wear does not depend on direction. $|t_i|$ is dependent on the friction coefficient, μ, therefore the change in wear depth per slice is sensitive to the friction coefficient. This means the frictional power wear model can give a more accurate prediction of wear in the roller/raceway contact, and it will be able to respond more appropriately to changes in the grease condition.

For each iteration of the feedback loop (see Figure 1), the wear profiles from the first roller encountered to the last roller encountered by the raceway (as the shaft and cage rotate) are summed for one revolution first, and then the acceleration factor is applied to this profile. Figure 6 shows an example of the wear accumulating on the inner race in the loaded zone over one revolution of the shaft.

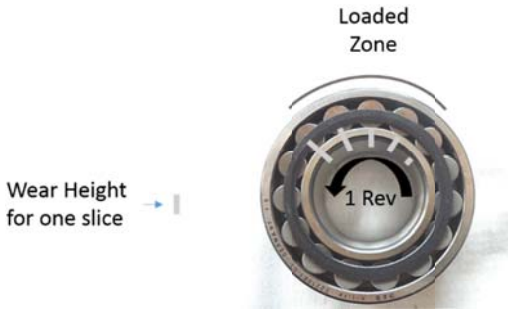

Figure 6. Diagram representing the accumulation of wear on the inner race from the contributions of each roller in one revolution. Wear accumulation is signified by the grey bars. (modified from (Wuxi Handa Bearing Co. Ltd 2016)) This figure shows that the wear on the inner race accumulates despite the varying loads it encounters as it passes the loaded zone.

This is performed by defining the code that determines the individual roller loads (based on the total radial load on the bearing) as a function that can be called during simulation. This means that it provides different individual roller loads depending on the total radial load on the bearing. The total radial load is able to varied as often as once per iteration (and this is affected by the acceleration factor). The bearing loads are generated and stored in a vector when the simulation is initialising, so that complicated loading patterns can be simulated (e.g. statistical variation). The outer race is assumed to be held loosely in the housing, allowing the wear to be uniformly distributed around the inner and outer raceways.

3. RESULTS

The thrust bearing model was run as a simulation with the parameters as in Table 1 and the results and descriptions can be seen in Sections 3.1 and 3.2.

Table 1. Parameters used in the thrust bearing simulation.

Parameter	Symbol	Value (thrust, radial)	Units
Coefficient of friction	μ	0.05	
Shear Modulus	G	79000	N/mm2
Poisson's Ratio	v	0.3	
Density of Steel	ρ	7800	kg/m^3
Length to centre of roller (thrust)		86.3	mm
Angle of roller to bearing axis (radial)		11.5	degrees
Inner Race radius (radial)		107.5	mm
Outer race radius (thrust, radial)		114, 104	mm
Roller radius (transverse)		109.5, 100	mm
Roller diameter (thrust, radial)		25.48, 19.7	mm
Roller width (thrust, radial)		30, 27.6	mm
Number of rollers (thrust, radial)	m	15, 22	
Number of slices along the roller		1000	
Axial load (Contact load tuned to) , Radial load (per side of bearing)		113000 (4153), 20000	N
(Dimensional) Wear coefficient	k, k_1	15×10^{-10}	mm2/N
Frictional Power wear coefficient	k_2	0.78×10^{-16}	kg/(N*mm)
Number of revolutions of the shaft per cycle pass (thrust, radial)		6000, 10 million	
Number of cycle passes (thrust, radial)		80, 50	

3.1 Final Wear Profile for the Thrust Bearing Model

The thrust bearing model was run, to compare with the results of Olofsson et al (Olofsson, Andersson, and Bjorklund 2000). A close approximation was able to be achieved to the experimental wear profile as shown in Figure 7.

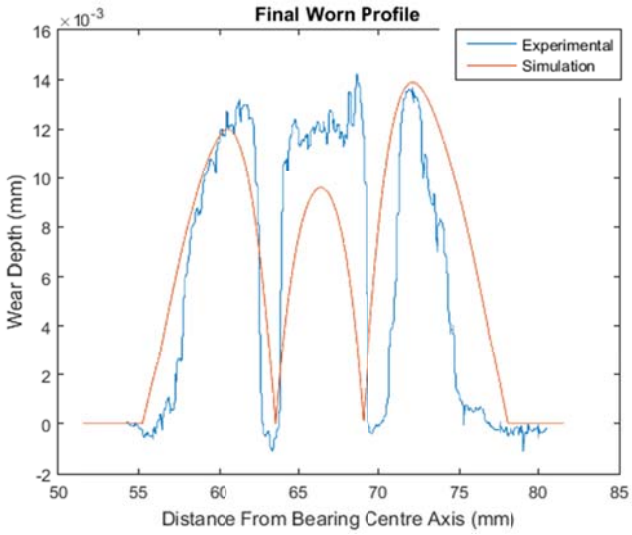

Figure 7. Experimentally measured wear profile from (Olofsson, Andersson, and Bjorklund) and thrust bearing simulation replicating Olofson et al's (Olofsson, Andersson, and Bjorklund) wear result, used for validation.

The simulated wear is asymmetrical but reasonably close to the experimental results. The creep in the contact culminates in a different traction force being applied to the roller depending on the position along the roller. The results show three peaks in wear. This is because there can be no net traction transmitted, and the outer positive (side peaks) and inner negative (middle peak) traction forces that depend on the creep (see for example Figure 8 A)) must cancel. The lines of no slip indicate the positions of zero tractional force, or pure rolling. As there is no sliding in pure rolling, there is little to no wear in these regions. The simulation result approximates the positions of these "zero-sliding" points well. The magnitude of the wear is similar to the magnitude of the measured wear profile, with deviations most likely caused by the nominal geometry used in the model. The simulated wear is smoother than the experimentally determined wear due to the idealised conditions of the model.

3.2 Initial Conditions and Final Wear Profile for the Radial Bearing Model

It is evident from Figure 8 A) that only the top five rollers (top roller; 2nd top and 3rd top rollers down each side) are loaded in the axle bearing for 20000 N (per side of the bearing).

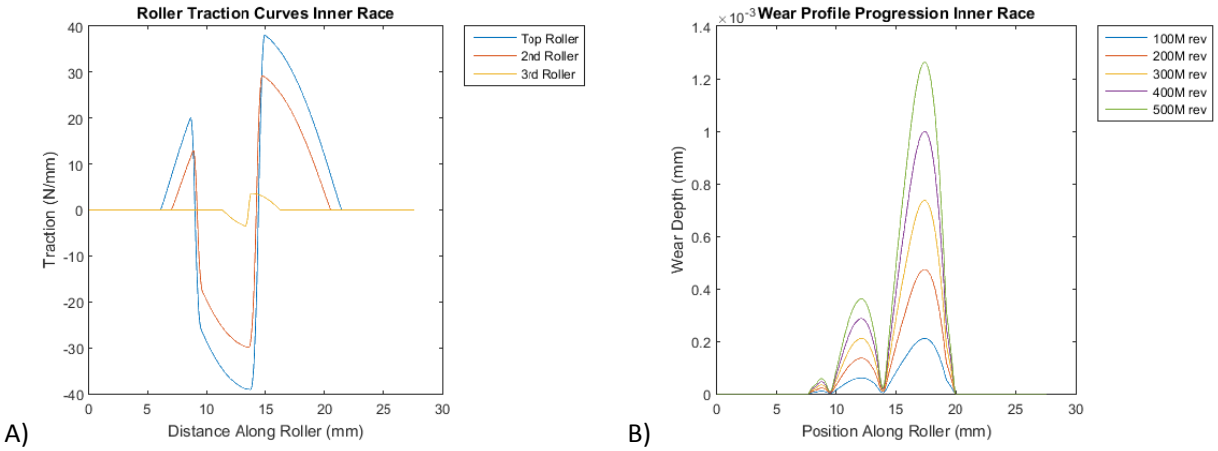

Figure 8. A) Traction curves for each roller for an applied load of 20000 N per side of the bearing. (This figure shows that the top roller has the most traction, this is due to the higher load it supports). B) The progression of wear in the simulation of the radial bearing. The horizontal axis in each figure represents the distance along the axis of the roller, starting from the outer end at 0 mm.

From Figure 8 B) it can be seen that there are three main peaks of wear, with little to no wear at the points of no-slip. Each colour represents the wear profile at that point in the life of the bearing. 500M revs translates to roughly 10 years of wear. The wear progresses evenly over life of the bearing. The traction and wear curves are asymmetrical, due to the fact that the rolling cone intersects the contact asymmetrically giving asymmetrical wear. It can be seen that the points of no slip in Figure 8 B) correlate well with the central intersections of the zero-traction line in Figure 8 A). This is due to the fact that where there is no traction, there is no sliding and thus, no wear.

4. CONCLUSIONS

A initial thrust bearing model of a spherical roller bearing has been compared to Olofsson et al's (Olofsson, Andersson, and Bjorklund 2000) article, and the simulation of the wear profile is reasonably close to the experimental profile. Using this model with some changes for the new geometry and radial loading, a prediction of the wear in a railway axle bearing (the radial bearing model) was able to be made with calculations of the load on each roller in the loaded zone of the bearing. This was performed along with predictions of the traction in the contact, all of which may be important for determining the lifetime of the bearing. This paper contributes to the literature by extending the models used by Olofsson et al (Olofsson, Andersson, and Bjorklund 2000) and Meehan et al (Meehan et al. 2009) to be used for radially loaded spherical roller bearings, as can be found in passenger train fleets. With this research, it is possible to determine the wear in the bearings, according to the frictional power wear formula, giving an indication of the life of the bearing.

ACKNOWLEDGEMENTS

This research is supported and made possible by the Rail Manufacturing CRC, Bombardier Transportation, NTN and the UQRS scholarship scheme.

REFERENCES

Archard, J. F. 1953. 'Contact and rubbing of flat surfaces', *Journal of Applied Physics*, 24: 981-88.

Changsen, W., and Z. Zhaoying. 1991. *Analysis of Rolling Element Bearings* (Mechanical Engineering Publications Limited: London).

El-Thalji, I., and E. Jantunen. 2014. 'A descriptive model of wear evolution in rolling bearings', *Engineering Failure Analysis*, 45: 204-24.

Johnson, K. L. 1960. "Tangential Tractions and Micro-slip in Rolling Contact." In *Rolling Contact Phenomena*, edited by J. B. Bidwell. Michigan: Elsevier.

Meehan, P. A., P. A. Bellette, R. D. Batten, W. J. T. Daniel, and R. J. Horwood. 2009. 'A case study of wear-type rail corrugation prediction and control using speed variation', *Journal of Sound and Vibration*, 325: 85-105.

Meehan, P. A., and W. J. T. Daniel. 2008. 'Effects of wheel passing frequency on wear-type corrugations', *Wear*, 265: 1202-11.

Nilsson, R., F. Svahn, and U. Olofsson. 2006. 'Relating contact conditions to abrasive wear', *Wear*, 261: 74-78.

Olofsson, U., S. Andersson, and S. Bjorklund. 2000. 'Simulation of mild wear in boundary lubricated spherical roller thrust bearings', *Wear*, 241: 180-85.

Palmgren, A. 1959. *Ball and Roller Bearing Engineering* (Philadelphia).

Wuxi Handa Bearing Co. Ltd. 2016. 'Spherical Roller Bearings', Accessed April 7. http://www.skf16.com/sale-104415-spherical-roller-bearings.html.